

CONDENSED MATTER PHYSICS

Electrically switchable ON-OFF spin-orbit torque in an ionic-gated metallic trilayer

Soobeom Lee^{1,2}†*, Suhyeok An¹, Eunchong Baek¹, Dongryul Kim¹, Jaeyong Cho¹, Chun-Yeol You¹*

With the advancement of magnetization-based spintronic applications, there has been considerable interest in spin-orbit torque as an electric technique to dynamically manipulate magnetization. In this study, gate-induced ON-OFF switchable spin-orbit torque in Pt/Co/Pt spin-orbit device using the ionic gating technique is reported. By canceling the spin currents from Pt layers, the OFF state is attained in Pt/Co/Pt spin-orbit device. Notably, under a strong negative gate electric field applied to the Pt/Co/Pt spin-orbit device, the damping-like spin-orbit torque is markedly enhanced over sixfold compared with the applied positive gate electric field. We show that the gate modulation of the spin-orbit torque in the Pt/Co/Pt spin-orbit device can be explained by considering the change of the spin-charge interconversion by electric gating. This research serves as a promising avenue for electrically programmable spintronic devices.

Copyright © 2025 The Authors, some rights reserved; exclusive licensee American Association for the Advancement of Science. No claim to original U.S. Government Works. Distributed under a Creative Commons Attribution NonCommercial License 4.0 (CC BY-NC).

INTRODUCTION

Electrically programmable spintronic devices are promising for the development of high-performance, low-energy-consumption logic and data storage (1). Electric field control of magnetization dynamics offers a scalable solution to realize the electrically programmable spintronic devices by exploiting a wide variety of physical phenomena in ferromagnetic materials, such as charge accumulation/depletion (2), magnetic phase transition (3), oxygen ion migration (4), and quadrupole induction of electronic orbitals (5). In addition, spin current absorption is a fascinating approach for manipulating magnetic moments by transferring the angular momentum of conduction electrons. For example, spin current can be generated by charge flow via spin-orbit coupling, which is a process that exerts the spinorbit torque (SOT) on the magnetic moment. SOT benefits from fast and energy-efficient magnetization switching (6-8), which is important in practical devices. A challenge in designing SOT-based devices is the modulation of SOT itself using the electric field effect because the applications of electric field control are restricted to semiconducting materials (9, 10) and a few unique platforms, such as topological insulators and lateral gate structures (11, 12). However, the important materials with large spin-orbit coupling are 5d heavy metals, such as Pt, Ta, and W (13-15). Hence, the realization of an electric field-tunable SOT device using heavy metals with large spin-orbit coupling greatly affects SOT physics and advanced SOTbased logic applications.

Despite the promising potential of electric field control in heavy metal-based SOT devices, its realization remains a substantial challenge because of its large carrier density and screening length, which is limited to a few atomic layers of metals. However, by using a gate dielectric with high capacitance per unit area in an ultrathin metallic system or magneto-ionic control through chemical migration, previously unexplored routes for modulating the SOT can be discovered. Moreover, the application of a strong electric field through solid and ionic gating techniques in ultrathin metallic systems has allowed for

¹Department of Physics and Chemistry, Daegu Gyeongbuk Institute of Science and Technology, Daegu 42988, Republic of Korea. ²Basic Science Research Center, Daegu Gyeongbuk Institute of Science and Technology, Daegu 42988, Republic of Korea. *Corresponding author. Email: sblee@shinshu-u.ac.jp (S.L.); cyyou@dgist.ac.kr (C.-Y.Y.) †Present address: Department of Electrical and Computer Engineering, Shinshu University, Nagano 380-8553, Japan.

innovations in condensed matter physics, such as strong modulation of the ferromagnetic phase in nanometer-thick Co films (4, 16-18), suppression of superconductivity in Al thin films (19), gate-tunable spin-charge interconversion in nanometer-thick Pt (20-22), and gate modulation of SOT (23-25). Thus, because a gate electric field contributes to the modulation of material properties, such as electrical conductivity and spin-charge interconversion, in the heavy metal layer, the SOT exerted on an adjacent ferromagnetic layer from the heavy metal layer can also be modulated.

RESULTS

Electric gating effect in Pt/Co/Pt

Here, we report the operation of a spin-orbit device that electrically switches the SOT on and off. The spin-orbit device involves a metallic trilayer system with a symmetric Pt/Co/Pt configuration and perpendicular magnetic anisotropy to efficiently modulate the SOT. SOT originating from the nominally identical bottom and top Pt layers inherently cancels each other out, indicating a completely off state of SOT (Fig. 1A). Moreover, gate voltage application induces the breaking of electric symmetry, resulting in asymmetric spin currents from the bottom and top Pt layers. Specifically, the spin current originating from the bottom Pt layer exerts a dominant torque on the magnetic moment of the ferromagnetic layer when the spin current from the top Pt layer is suppressed by applying a gate voltage (Fig. 1B); the opposite phenomenon can also be observed (Fig. 1C). Reportedly, the spin-charge interconversion efficiency in Pt can be tuned by electric gating through charge density modulation or hydrogen adsorption (20, 22). In this manner, an inherently net-zero SOT can be electrically activated by the applied gate voltage, enabling an electrically switchable ON-OFF SOT. To accomplish the operation of the spin-orbit device, an ionic gating technique using an electrolyte is used. When a gate voltage is applied to the gate/electrolyte/channel structure, the cations and anions of the electrolyte are polarized by the gate electric field, and the polarized ions could induce the charge doping and/or hydrogen absorption or adsorption via electrolysis on the channel surface.

The magnitude of the current-induced SOT on the magnetic moment (**m**) can be represented by effective magnetic fields—longitudinal effective field $(H_{\rm DL} \alpha | \mathbf{m} \times \mathbf{\sigma}|)$ of the anti–damping-like (DL)–SOT

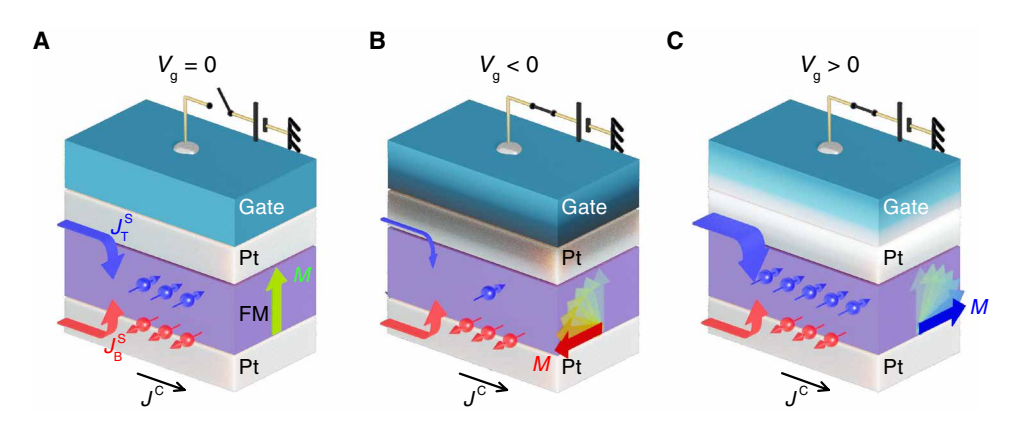


Fig. 1. Conceptual schematic of the electrically ON-OFF switchable SOT in the spin-orbit device. (A) In the symmetric Pt/ferromagnetic material (FM)/Pt trilayer, spin currents generated from the top and bottom Pt layers cancel each other out, resulting in a net-zero SOT (OFF state). (B and C) When a gate voltage is applied, if the spin current from the top Pt layer is suppressed or enhanced, then the finite SOT reaches the FM layer (ON state).

mostly created by the spin Hall effect (26, 27) and the transverse effective field ($H_{\rm FL} \propto |\sigma|$) of the field-like (FL)–SOT mostly created by the Rashba-Edelstein effect (28, 29)—where $\sigma = \mathbf{j} \times \mathbf{z}$, \mathbf{j} and \mathbf{z} are unit vectors in the current and out-of-plane directions, respectively. The well-established harmonic Hall method using ac is a very suitable approach for quantifying the magnitudes of effective fields of SOT (30–32). The effective fields of DL-SOT (FL-SOT) are determined by analyzing the second harmonic Hall voltages with planar Hall correction under longitudinal (transverse) applied external magnetic fields (30). The advantage of this method is that it provides separate DL-and FL-SOT effective fields, making it suitable for the analysis of gate-tunable SOT systems.

Figure 2A shows the structure of a gate-tunable spin-orbit device consisting of Pt (2 nm)/Co (1 nm)/Pt (1.5 nm) with a 0.5-nm-thick Ta buffer layer on a SiO2 substrate. Notably, DL-SOT induced by the spin currents from 2-nm Pt (bottom) and 1.5-nm Pt (top) shows almost net-zero SOT, despite their different thicknesses (see Fig. 2E). We speculate that the cancellation arises because of the intrinsic differences in growth conditions for the top and bottom Pt layers. Additional details are provided in section S7. A Ta buffer layer is grown to enhance the crystal quality and perpendicular magnetic anisotropy. As shown in Fig. 2D, clear hysteresis of the anomalous Hall effect is observed as a manifestation of perpendicular magnetic anisotropy in the Pt/Co/Pt trilayer. For gate voltage (Vg) application, an ionic gel consisting of a mixture of the diethylmethyl(2-methoxyethyl) ammonium bis(trifluoromethylsulfonyl)imide (DEME-TFSI) electrolyte and polystyrene-polymethyl methacrylate-polystyrene (PS-PMMA-PS) polymer is applied in the side-gate geometry (Materials and Methods). V_g is swept from +2 V to -2 V at atmospheric condition and room temperature, where the ions of the electrolyte are mobile. The cations and anions are polarized near the surface of the channel, as shown in Fig. 2B. We note that the electrochemical window of DEME-TFSI is known to exceed 2 V, suggesting that the electrochemical reactions of the electrolyte itself are prevented in our experiments (33, 34). In addition, the ac current flowing through the capacitive ionic gate could influence the ionic structure. Because the polarized ions in the electrolyte are frozen below the glass transition temperature, harmonic Hall measurements are conducted at 200 K to retain the ionic structure (20, 35). As shown in Fig. 2C, the longitudinal resistance (R_{xx}) is altered by applying V_g . A change in R_{xx} of ~10%

of the resistance for the pristine device is observed, implying that the charge density or charge-carrier scattering is modulated by electric gating. Notably, the characteristic hysteresis in the $V_{\rm g}$ dependence is shown, which will be discussed later.

Modulation of SOT through electric gating

The first and second harmonic Hall signals $(V_{xy}^{\ \omega}, V_{xy}^{\ 2\omega})$ for the longitudinal (||) and transverse (\bot) external magnetic fields are measured as a function of the applied magnetic field, respectively. Figure 2 (E and F) shows that $V_{xy,\parallel}^{\ 2\omega}$ is almost constant for the pristine sample regardless of the applied magnetic field, while $V_{xy,\perp}^{\ 2\omega}$ has a linear relationship with a finite slope. These findings imply that DL-SOT is approximately zero. Specifically, the spin Hall currents from the top and bottom Pt layers completely cancel out despite their different thicknesses. Unlike DL-SOT, with the observed $V_{xy,\perp}^{\ 2\omega}$, it seems likely that asymmetric interfacial spin-orbit couplings for the top and bottom layers give rise to FL-SOT.

Having outlined the initial conditions, we conduct harmonic Hall measurements by first applying $V_{\rm g}$ from 2 to -2 V and subsequently from -2 to 2 V. To ensure that the SOT contribution is linearly proportional to the applied current, the amplitude of the electric ac is varied from 2 mA $(0.4 \times 10^{11} \text{ A m}^{-2})$ to 5 mA $(1 \times 10^{11} \text{ A m}^{-2})$ A m⁻²). Figure 3 presents a summary of the investigation of harmonic Hall measurements with electric gating. Figure 3 (A, B, D, E, G, H, J, and K) shows the first- and second-harmonic Hall voltages. The solid lines represent parabolic fits for the first-harmonic Hall voltages and linear fits for the second-harmonic Hall voltages. $\mu_0 H_{\rm DL}$ and $\mu_0 H_{\rm FL}$ are extracted from harmonic Hall signals through planar Hall correction, where μ_0 is the magnetic permeability under vacuum conditions (section S3). Figure 3 (C, F, I, and L) shows the current density dependences of $\mu_0 H_{DL}$ and $\mu_0 H_{FL}$ in both the upmagnetization (+M) and down-magnetization (-M) states at applied V_g values of +2, 0, -2, and 0 V, respectively. The measurements are conducted sequentially over time. Linear relationships between the effective fields and the amplitude of the ac imply that harmonic Hall signals are dominated by SOT contributions rather than by thermoelectric contributions due to Joule heating. We focus on how efficiently SOT is generated depending on the applied current amplitude. The SOT efficiency of DL-SOT (FL-SOT), $\xi_{DLT(FLT)}$, is described as follows

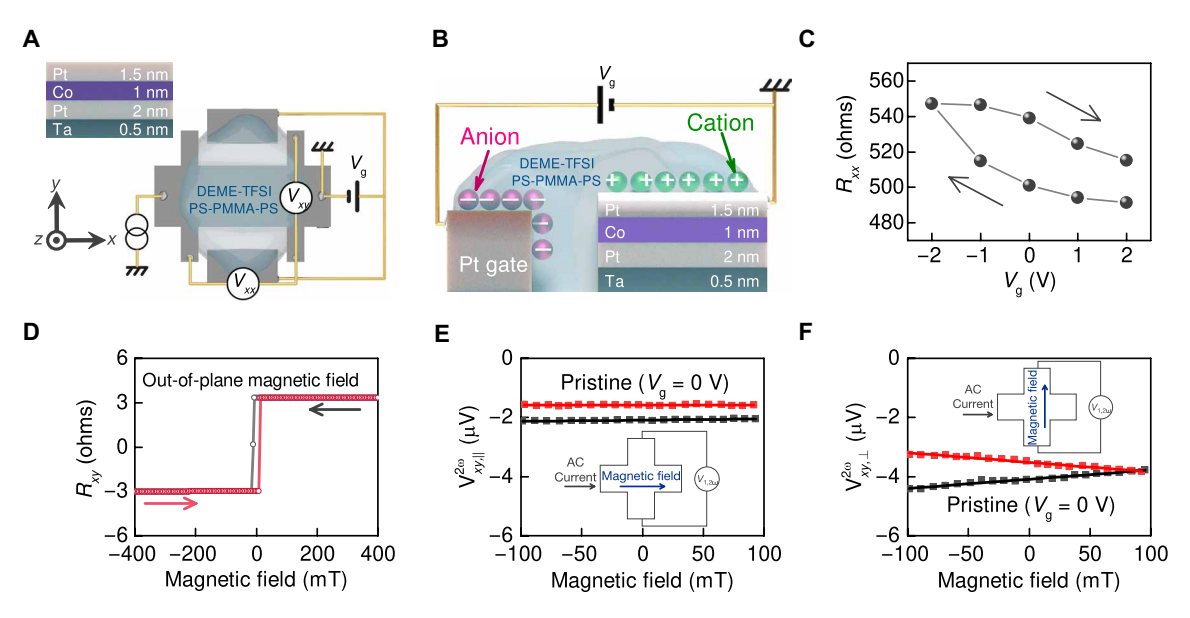


Fig. 2. Device structure and basic characteristics of a Pt/Co/Pt spin-orbit device. (A) Schematic image of a metallic trilayer Hall bar device made of Pt/Co/Pt with a Ta buffer layer. To apply a gate voltage, an ionic gel based on DEME-TFSI is applied with a side gate configuration. Longitudinal (V_{xx}) and transverse (V_{xy}) voltages are measured in the Hall bar device. (B) Schematic description of the ionic gating technique in the side gate geometry. The anions, which are cations of the electrolyte, are polarized by the gate electric field. (C) Longitudinal resistance of the Hall bar device as a function of gate voltage (V_g) . V_g is swept between ± 2 V. (D) Typical hysteresis of the anomalous Hall resistance when an out-of-plane magnetic field is applied as a manifestation of perpendicular magnetic anisotropy. (E and F) Second harmonic Hall voltages versus applied magnetic field in the pristine device before applying V_g . An external magnetic field is applied along the longitudinal direction (E) and transverse direction (F). The black and red dots indicate the magnetization states $(\pm M)$ of the ferromagnetic layer pointing along $\pm z$ and $\pm z$, respectively. The solid lines are linear fits.

$$\xi_{\rm DLT(FLT)} = \left(\frac{2e}{\hbar}\right) \frac{t_{\rm F} \mu_0 M_{\rm s} H_{\rm DL(FL)}}{I^{\rm C}} \tag{1}$$

where e is the elementary charge, $M_s = 1 \text{ kA/m}$ is the saturation magnetization measured by the vibrating sample magnetometer, $t_{\rm F}$ is the thickness of the ferromagnetic layer, \hbar is the Dirac constant, J^{C} is the amplitude of the ac, $(2e/\hbar)$ is the conversion from spin angular momentum to electrical charge, and $t_{\rm F}\mu_0 M_{\rm s} H_{\rm DL(FL)}$ is the spin angular momentum per unit area that induces DL-SOT (FL-SOT). $\xi_{DLT(FLT)}$ is calculated using Eq. 1 and the linear slope of effective field versus applied current density at each applied $V_{\rm g}$. The complete dataset of $\xi_{DLT(FLT)}$ as a function of V_g is shown in Fig. 4A, and a prominent change in $\xi_{DLT(FLT)}$ is observed, which depends on the applied $V_{\rm g}$. An inherently negligible $\xi_{\rm DLT}$ changes sign under a positive gate voltage application. The change in the sign implies that the SOT created by the spin Hall effect in the top Pt layer becomes dominant. When a negative gate voltage is applied, more surprisingly, ξ_{DLT} markedly increases to 0.066, which is comparable to ξ_{DLT} in a Pt/Co system without a top metal layer (36). The positive sign of $\xi_{\rm DLT}$ indicates the dominant contribution from the bottom Pt layer, highlighting the suppression of DL-SOT from the top Pt layer. Given that the magnitude of ξ_{DLT} is close to 0 at an applied V_g of +2 V and increases by more than 0.06 at an applied V_g of -2 V, it can be inferred that SOT exhibits sensitivity to the applied $V_{\rm g}$. The observed modulation ratio $[|\xi_{DLT}(-2 \text{ V})/\xi_{DLT}(+2 \text{ V})|]$ of 633% through ionic gating in our Pt/Co/Pt spin-orbit device is large, demonstrating the ON-OFF operation of the SOT efficiencies in the spin-orbit device. Furthermore, the observed results demonstrate greater gate modulation ratio than those of previous studies using topological insulators, lateral gating systems, and magneto-ionic control (11, 12, 23,

25). To obtain intuitive insight into the ionic gating effect, $\xi_{\text{DLT}(\text{FLT})}$ is plotted as a function of R_{xx} . There is hysteresis in the V_{g} dependence of $\xi_{\text{DLT}(\text{FLT})}$, as shown in Fig. 4A, similar to the V_{g} dependence of R_{xx} in Fig. 2C. We can plot $\xi_{\text{DLT}(\text{FLT})}$ as a function of R_{xx} , which presents distinct and clear dependencies, as shown in Fig. 4 (B and C). While ξ_{FLT} is weakly nonlinear in R_{xx} and the modulation ratio is not very large, ξ_{DLT} demonstrates an approximately linear relationship with R_{xx} . Considering the evident trends of ξ_{DLT} and ξ_{FLT} with respect to R_{xx} , it is reasonable to speculate that changes in SOT efficiencies are closely related to electronic transport. Because of the difficulty in interpreting the FL-SOT, which arises primarily due to the complexity associated with the contribution from the Oersted field, we exclusively examine the DL-SOT induced by the spin Hall effect in the subsequent sections.

DISCUSSION

First, we phenomenologically discuss the electric gating mechanism on the basis of the experimental results in our system. The charge doping via the electric double layer and chemical migration through electrolysis have been reported in the ionic gating systems. In the case of the ionic effect through electrolysis, H_2O in the atmosphere or electrolyte plays a crucial role. In our experiments, the gate voltage was applied under atmospheric conditions and at room temperature, allowing hydrogen ions generated from atmospheric water to adsorb or absorb onto the Pt surface. We performed R_{xx} - V_g measurements under both atmospheric and vacuum condition and found that R_{xx} is not modulated in a vacuum (section S9). This observation suggests that the dominant gating mechanism in our experiments is likely attributable to the ionic effect rather than the

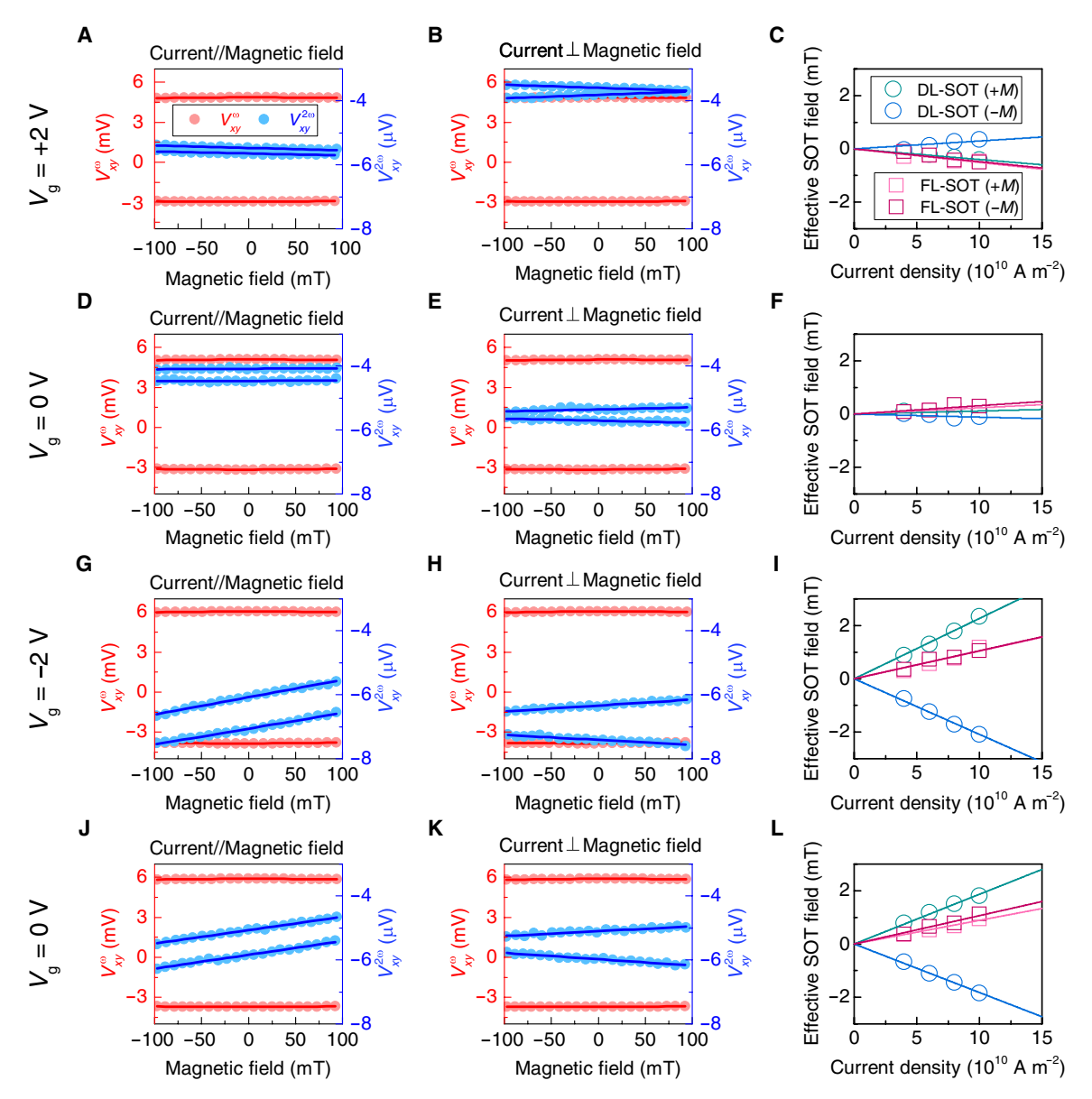


Fig. 3. Harmonic Hall measurements and effective magnetic fields. First and second harmonic Hall voltages when (A, D, G, and J) the current direction is parallel to the magnetic field and (B, E, H, and K) the current direction is perpendicular to the magnetic field. (C, F, I, and L) Effective magnetic fields as a function of current density and gate voltage V_g . The V_g values were set to +2, 0, -2, 0, and +2 V, respectively. The green and blue circles indicate DL-SOT for +M and -M, respectively. The solid lines are linear fits.

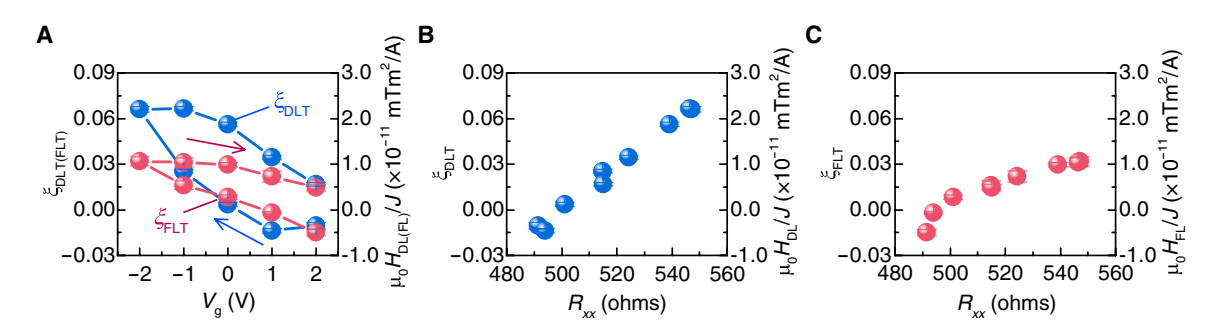


Fig. 4. Gate modulation of the effective fields of the SOT. (A) V_g dependence of the efficiencies of DL-SOT and FL-SOT. The blue and red circles indicate DL-SOT and FL-SOT, respectively. (B and C) Efficiencies of (B) DL-SOT and (C) FL-SOT as a function of the longitudinal resistance (R_{xx}).

conventional electric field effect of the electric double layer. In this mechanism, the gating effect can persist even after the gate voltage is turned off, and hysteresis behavior observed in the experimental results is attributable to this, enabling potential applications in non-volatile memory and logic devices.

As an ionic effect via electrolysis, two potential mechanisms can be considered: a bulk effect mediated by proton transport and a surface effect driven by hydrogen adsorption/desorption. In the case of the bulk effect, the gating phenomenon is not restricted to the surface but could extend to influence the entire structure. Previous studies have documented significant voltage control of magnetic anisotropy (VCMA) through proton (H⁺) migration, where H⁺'s are generated via the hydrolysis of H₂O and transported through a Grotthuss-type mechanism (18, 37). On the other hand, the study of hydrogen adsorption on Pt surfaces has been a prominent research topic for nearly a century. Recent findings have demonstrated that hydrogen ions can be electrically adsorbed and desorbed on ionicgated Pt surfaces, thereby modulating spin-charge conversion (22).

To discern whether the gate modulation of SOT observed in our experiments originates from the bulk effect or the surface effect, we examined VCMA simultaneously during the main experiment using the same device structure, Ta(0.5 nm)/Pt(2 nm)/Co(1 nm)/Pt(1.5 nm). Because the ferromagnetic Co layer is not located at the surface, we hypothesize that its magnetic anisotropy would be more sensitive to the bulk effect induced by ionic gating. The first-order perpendicular magnetic anisotropy fields ($H_{\rm K1}^{\rm eff}$) are extracted using the generalized Sucksmith-Thompson method (section S8). As shown in Fig. 5, $H_{\rm K1}^{\rm eff}$ is modified by ~80 mT when the gate voltage is varied between ± 2 V. In contrast to the severalfold modulation of the DL-SOT, the modulation of $H_{\rm K1}^{\rm eff}$ is relatively small, amounting to only about 10%. This finding strongly suggests that the electric gating on SOT efficiency is predominantly governed by the surface effect of hydrogen adsorption/desorption.

The modest change in magnetic anisotropy field can be attributed to several factors, including the spin-polarized Pt layer induced by

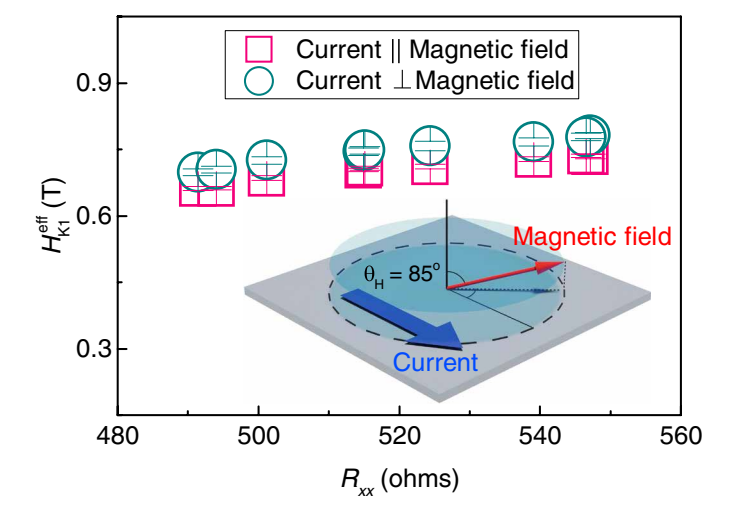


Fig. 5. Gate modulation of effective anisotropy field. Effective magnetic anisotropy field as a function of longitudinal resistance. Anisotropy field is evaluated by the generalized Sucksmith-Thompson method. Purple squares and green circles indicate measurements with parallel- and perpendicular-magnetic field direction to the current direction.

the magnetic proximity effect and magneto-ionic gate control via proton transport. A nonmagnetic Pt layer adjacent to the ferromagnetic layer can become spin-polarized through the magnetic proximity effect (38-40). Furthermore, recent studies indicate that the spin-polarized region in Pt due to this effect can extend over a thickness of 1 nm (41-44). Even if the gating effect is primarily confined to the Pt surface, we speculate that the partially spin-polarized Pt layer near the surface could still be influenced by electric gating. As previously reported, changes in magnetic anisotropy can also arise from gate-induced ionic migration (18, 25, 37). The limited change in magnetic anisotropy observed in our experiments is likely a consequence of the extremely low solubility of hydrogen in Pt (45).

Although hydrogen adsorption/desorption on the Pt surface is likely the primary mechanism driving the ionic gating effect observed in our experiments, the associated changes in the electrical resistance of the device present an intriguing phenomenon. Previous studies have reported reductions in both the work function and electrical resistivity of Pt under hydrogen-rich environments (46). Furthermore, early theoretical investigations suggested that hydrogen adsorbed on the Pt surface contributes conduction electrons, thereby altering its electronic properties (47). These findings indicate that ionic gating-induced hydrogen adsorption/desorption could directly modulate the electrical resistance of Pt. This observation is consistent with our hypothesis that surface effects play a pivotal role in the investigated phenomena. Notably, while this mechanism differs from the conventional electric field effect, it still involves charge density modulation facilitated by hydrogen adsorption/desorption.

We now discuss the electric modulation of SOT. As mentioned above, hydrogen adsorption and desorption induced by gating could alter the charge density. This change in charge density may, in turn, affect the SOT dynamics. Conceivable explanations for the electric modulation of DL-SOT through ionic gating are as follows. (i) Under the applied positive V_g , the resistance near the surface decreases because of electric gating, resulting in variations in the current distribution. The opposite trend is also apparent. Specifically, the reduction in the electric current in the top Pt layer under the applied negative V_g results in the dominant SOT originating from the bottom Pt layer. (ii) In addition to the influence described in (i), the spin-charge interconversion efficiency in the top Pt layer can be modulated by the electric gating (20-22). If the efficiency of spin current generation in the top Pt layer changes through electric gating, then it changes the magnitude of the SOT applied to the ferromagnetic layer. As calculated by Eq. 1, ξ_{DLT} is dependent on M_s in the ferromagnetic layer. Because the modification of the magnetic anisotropy is not large enough to corroborate the experimentally obtained modulation of ξ_{DLT} , as shown above, we exclude the contribution of the modification of M_s in the ferromagnetic layer being influenced by an electric gating.

To understand the mechanism by which the SOT in Pt/Co/Pt spin-orbit device is modulated by electric gating, we consider a simple trilayer (heavy metal–ferromagnetic–heavy metal) model (Fig. 6A), where the top and bottom layers of the heavy metal and ferromagnetic layers are represented as T, B, and F, respectively, in the mathematical description. The current density and resistivity before the electric gating are initially assumed to be uniform. Assuming that only the resistance of the top heavy metal layer changes due to the electric gating, we calculate the current density in each layer based on the change in R_{xx} when a gate voltage is applied. By solving the phenomenological spin diffusion equation in the presence of

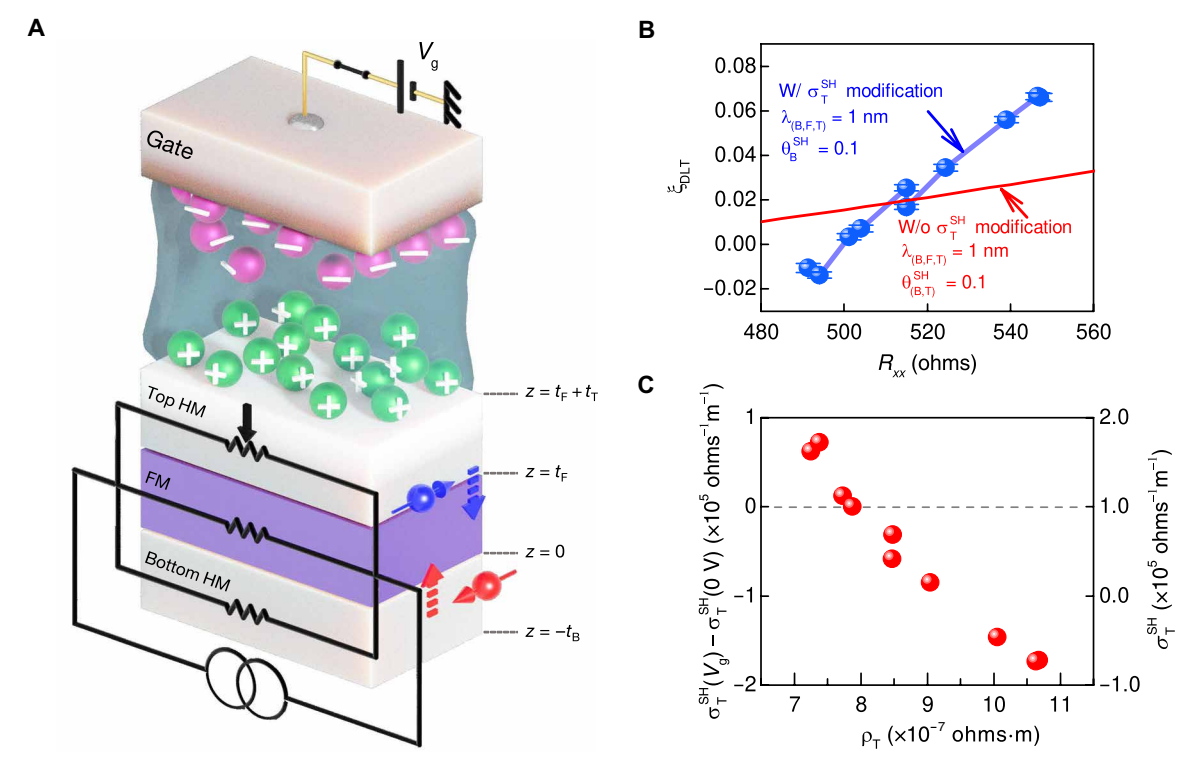


Fig. 6. Underlying physics of gate modulation of DL-SOT efficiency. (**A**) Schematic illustration of the heavy metal (HM)/ferromagnetic material (FM)/HM trilayer for the spin diffusion model calculation. The trilayer configuration conducts the current in parallel, where the total electric current density is J^{C} . Only the resistivity (ρ_{T}) and spin Hall conductivity (σ^{SH}_{T}) of the top HM layer are influenced by the gate electric field. (**B**) Efficiency of DL-SOT calculated by the parallel resistance model and spin diffusion equation as a function of R_{xx} . The red solid line indicates the trend expected without modification of σ^{SH}_{T} , while the semitransparent blue solid line is calculated to replicate the experimental results considering gate-tuned σ^{SH}_{T} . The blue circles are the experimentally obtained DL-SOT efficiencies. (**C**) Variation in σ^{SH}_{T} , which is determined to enable the spin diffusion equation–based parallel resistance model to reproduce the experimental results, as a function of ρ_{T} .

the spin current generated by the spin Hall effect, we subsequently analytically calculate the spin-dependent current in each layer. As shown in Fig. 6A, spin currents are generated from the top and bottom heavy metal layers via the spin Hall effect. The spin angular momentum of the spin current is converted into torque in the magnetic moments of the ferromagnetic layer through the spin relaxation process. From this perspective, the DL-SOT efficiency can be defined as the overall change in spin current originating from the spin Hall effect in the ferromagnetic layer with respect to the applied charge current (48, 49)

$$\xi_{\text{DLT}} = \frac{1}{J^{\text{C}}} \int_{0}^{t_{\text{F}}} \nabla J_{\text{F}}^{\text{S}}(z) dz \tag{2}$$

where J^{C} and J^{S}_{F} are the total charge current density and the spin current density for the ferromagnetic layer, respectively. By incorporating appropriate boundary conditions and assuming transparent interfaces, which simplify the model calculation, the theoretical description of the efficiency of DL-SOT is as follows

$$\begin{split} \xi_{\text{DLT}} &= \frac{1}{f^{\text{C}}} \\ &\left\{ \frac{r_{\text{B}} r_{\text{F}} J_{\text{B}}^{\text{SH}} T_{\text{T}} \left[1 - \text{sech} \left(\frac{t_{\text{B}}}{\lambda_{\text{B}}} \right) \right] - r_{\text{T}} r_{\text{F}} J_{\text{T}}^{\text{SH}} T_{\text{B}} \left[1 - \text{sech} \left(\frac{t_{\text{T}}}{\lambda_{\text{T}}} \right) \right]}{\sinh \left(\frac{t_{\text{F}}}{\lambda_{\text{F}}} \right) \left[4 r_{\text{B}} r_{\text{T}} + \left(\frac{r_{\text{F}}}{2} \right)^{2} \tanh \left(\frac{t_{\text{B}}}{\lambda_{\text{B}}} \right) \tanh \left(\frac{t_{\text{T}}}{\lambda_{\text{T}}} \right) \right] + 4 r_{\text{F}} \cosh \left(\frac{t_{\text{F}}}{\lambda_{\text{F}}} \right) \left[r_{\text{T}} \tanh \left(\frac{t_{\text{B}}}{\lambda_{\text{B}}} \right) + r_{\text{B}} \tanh \left(\frac{t_{\text{T}}}{\lambda_{\text{T}}} \right) \right] \right\} \end{split}$$

$$(3.4)$$

$$T_{i} = -\tanh\left(\frac{t_{i}}{\lambda_{i}}\right) + 4\frac{r_{i}}{r_{F}}\sinh\left(\frac{t_{F}}{\lambda_{F}}\right) + \tanh\left(\frac{t_{i}}{\lambda_{i}}\right)\cosh\left(\frac{t_{F}}{\lambda_{F}}\right)$$
(3B)

where $r_F = 4\lambda_F \rho_F/(1 - P^2)$ and $r_{(T,B)} = \lambda_{(T,B)} \rho_{(T,B)}$ are the characteristic spin resistances; $\lambda_{(T,F,B)}$ is the spin diffusion length; $\rho_{(T,F,B)}$ is the electrical resistivity for T, F, and B, respectively; $J^{SH}_{(T,B)}$ is the spin Hall current defined by $J^{C}_{(T,B)}\theta^{SH}_{(T,B)}; J^{C}_{(T,B)}$ is the charge current density; $\theta^{SH}_{(T,B)}$ is the spin Hall angle for T and B; T_i is the effective spin absorption to layer i = T and B; and P is the spin polarization of F. The red solid line in Fig. 6B depicts the calculated ξ_{DLT} based on Eqs. 3A and 3B without considering modification of the spin Hall angle as a function of R_{xx} . The variation in the calculated ξ_{DLT} for $\lambda_{(T,E,B)}=1$ nm and $\theta^{SH}_{(T,B)}=0.1$, represented by the red solid line, is not as significant as that observed in the experimentally observed R_{xx} dependence of ξ_{DLT} (depicted by the blue circles in Fig. 6B). Even under extreme conditions for $\lambda_{(T,F,B)} = 0.2$ nm and $\theta^{SH}_{(T,B)} = 0.2$, as described in section S6, the calculation does not sufficiently replicate the experimental results. Hence, consideration of the gatetunned spin Hall angle in the spin diffusion model is essential to corroborate the electric field control of DL-SOT in the trilayer system, as presented in (20-22).

Figure 6C shows the R_{xx} dependence of the spin Hall conductivity ($\sigma^{\text{SH}} = \theta^{\text{SH}}/\rho$) of the top Pt layer for reproducing the experimental results. The ξ_{DLT} is calculated to reproduce the experimental

results, and it is represented by the semitransparent blue solid line in Fig. 6B. The model includes the effect of the electric field on ρ_T and θ^{SH}_{T} , while $\lambda_{(T,F,B)} = 1$ nm and $\theta^{SH}_{B} = 0.1$ are constant. The spin Hall conductivity is suppressed with increasing resistance, i.e., decreasing charge density via hydrogen desorption. In high-resistivity Pt $(\rho > 2 \times 10^{-7} \text{ ohms·m})$, the spin Hall effect is reported to be dominated by an intrinsic mechanism (50). Given that the resistivity in our experiment exceeds 7×10^{-7} ohms·m, the intrinsic spin Hall effect is confirmed. The intrinsic spin Hall effect can be intuitively described by electron excitation in the d-orbitals. When the electron travels through the inter-d-orbitals, the Berry phase creates an effective magnetic flux that gives rise to the spin Hall effect (51, 52). Thus, the spin Hall conductivity exhibits a significant correlation with the spin-orbit polarization for the d-band (53). In our experimental system, the applied gate voltage modulates the charge density via the hydrogen adsorption and desorption, resulting in a shift in the Fermi level and a modification of the electrical resistivity. Consequently, the spin Hall conductivity can be scaled depending on spin-orbit polarization for the d-band at the shifted Fermi level. According to the band calculation of the intrinsic spin Hall effect in Pt, it has been reported that the spin Hall conductivity strongly decreases below the Fermi level (54), which is consistent with the results of our experiment. Ultimately, the suppression of the spin-charge interconversion in the top Pt layer at the negative gate voltage leads to finite and significant DL-SOT, where the contribution from the bottom Pt layer is dominant.

We also discuss the opposite tendency of the gate modulation of spin-charge conversion reported in (20), where the spin-charge conversion of Pt ultrathin film on YIG is suppressed under an applied positive gate voltage. Because YIG is a ferrimagnetic insulator, no charge transfer occurs between the freestanding Pt and YIG. We hypothesize that the Fermi level in freestanding Pt is just above the energy level of maximum spin Hall conductivity, leading to the suppression of the spin-charge conversion under positive gate voltage. In contrast, in the Pt/Co/Pt trilayer used in our study, the top Pt layer is in contact with the metallic ferromagnetic layer, inducing charge transfer. This charge transfer may result in a downshift of the

Fermi level, potentially placing it below the energy level of maximum spin hall conductivity. Consequently, the spin-charge conversion could show an opposite behavior compared to the freestanding Pt case, as observed in our experiments.

Last, we verify the reproducibility of the electrically switchable operation of DL-SOT in the spin-orbit device using a different device with the same structure. To evaluate the magnitude of the DL-SOT, harmonic Hall analysis is repeated by alternatingly applying gate voltages between +2 and -2 V to devices with the same configuration. Figure 7 (A to F) shows the current density dependences of the effective fields of DL-SOT, and the measurements are carried out in sequence. The DL-SOT is repeatedly switched on and off by applying negative and positive gate voltages, respectively. This finding confirms that the gate-tuned ON and OFF states of DL-SOT are reversible and reproducible. For a quantitative representation, the applied gate voltage and the efficiency of DL-SOT are plotted in Fig. 7G as a function of the sequence of gate voltage application (n). When gate-tuning of the ON-OFF states of ξ_{DLT} in the spin-orbit device is successfully achieved, a time-dependent increase in ξ_{DLT} is observed. Time-dependent increases in the resistivity and SOT efficiency can be observed, even in the main experimental results. This result is elucidated by the characteristic self-organization of ions at the surface between the channel and ionic gel. A previous study reported that TFSI anions can self-organize in a treated graphene field effect transistor (34). Similarly, we speculate that TFSI anions are self-organized because of the repetitive freezing and melting of the ionic gel during the measurement process, which could result in a degradation of electrolysis efficiency. Despite the slight irreversible reaction in the electric gating, we emphasize that the clear trends of physical phenomena as a function of R_{xx} (Fig. 4, B and C) unambiguously support our claim that gate modulations of SOT in Pt/Co/ Pt spin-orbit device are related to the electronic transport.

In summary, our findings demonstrate gate modulation of SOT efficiencies in the ionic-gated Pt/Co/Pt spin-orbit device with an on/off ratio exceeding sixfold. The inherently dissipated DL-SOT in the symmetric Pt/Co/Pt trilayer is markedly enhanced by the suppression of the spin-charge interconversion through electric gating.

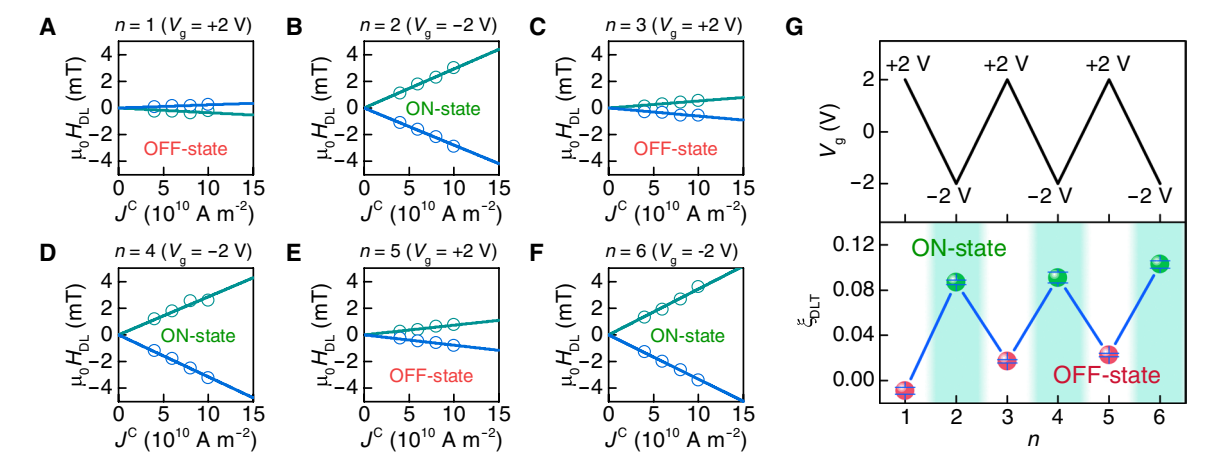


Fig. 7. Gate-induced ON-OFF switchable DL-SOT in the spin-orbit device through ionic gating. (A to F) Gate-modulated effective magnetic fields of DL-SOT as a function of the applied current density $\int_{-\infty}^{\infty} n$ is the sequence number of gate voltage applications. The gate voltage V_g is applied alternatively between +2 V (A, C, and E) and -2 V (B, D, and F). The green and blue circles indicate the effective fields for the +M state and -M state, respectively. The solid lines are the linear fits. (G) Input gate voltages and output DL-SOT efficiency. The top panel is the sequence of V_g application, and the bottom panel is the experimentally obtained DL-SOT efficiency after V_g application. In the bottom panel, the green-colored regions indicate the ON-states of DL-SOT.

Consequently, the performance of our demonstrated spin-orbit device surpasses that of other material systems using the topological insulator and lateral gating, establishing a previously unexplored branch of the electrically programmable spintronic devices. In addition, our platform provides an approach for studying gate modulation in fundamental physical phenomena related to spin-orbit coupling, such as the spin Hall effect and the Rashba-Edelstein effect.

MATERIALS AND METHODS

Sample fabrication

A thin film stack of Ta (0.5 nm)/Pt (2 nm)/Co (1 nm)/Pt (1.5 nm) was deposited on thermally oxidized silicon (100) substrates by dc magnetron sputtering. A Ta buffer layer was inserted to enhance the crystallinity and perpendicular magnetic anisotropy. A 10- μ m-wide Hall bar device and side gate electrodes were fabricated via standard photolithography and argon-ion milling. A layer of photoresist was applied using spin coating after device fabrication, and a window was subsequently exposed to apply a gate voltage efficiently to uncover the active area of the device and side gate electrode.

Ionic gating technique

An ion gel was prepared using a mixture with a DEME-TFSI:PS-PMMA-PS polymer:ethyl propionate weight ratio of 9.5:0.5:20. An ion gel (30 μ l) was applied to the Hall bar device. A gate voltage was applied using a Keithley 2400 at room temperature because the cations and anions in the ionic gel were mobile. In the harmonic Hall measurements, an ac was applied to the device. Because the ion distribution in the ionic gel could be influenced by the ac, the measurements were carried out at 200 K. After the measurements, the temperature was set to 300 K to apply the gate voltage again. The above measurement routine was repeated during the experiments.

Harmonic Hall measurements

We performed harmonic Hall measurements at 200 K in the cryostat. An ac current with an amplitude of 2 to 5 mA and a frequency of 113.3 Hz was applied using a Keithley 6221 in the harmonic Hall measurements. An external longitudinal and transverse magnetic field was applied within the plane. The first and second harmonic Hall voltages were simultaneously measured using two SR830 lockin amplifiers.

We have conducted additional measurements demonstrating that the gate modulation of SOT efficiency is effective even at room temperature. Using anomalous Hall shift measurements under an applied dc current (55), we confirmed a significant modulation of SOT efficiency at room temperature and atmospheric condition. While these findings are promising, a direct comparison with the harmonic Hall results presented in the modulation of SOT through electric gating section of the Results is not straightforward, as they belong to a follow-up research theme. These issues need to be clarified in more detailed future studies.

Supplementary Materials

This PDF file includes: Sections S1 to S9 Figs. S1 to S10 References

REFERENCES AND NOTES

- C. Song, B. Cui, F. Li, X. Zhou, F. Pan, Recent progress in voltage control of magnetism: Materials, mechanisms, and performance. *Prog. Mater. Sci.* 87, 33–82 (2017).
- D. Chiba, M. Sawicki, Y. Nishitani, Y. Nakatani, F. Matsukura, H. Ohno, Magnetization vector manipulation by electric fields. *Nature* 455, 515–518 (2008).
- R. O. Cherifi, V. Ivanovskaya, L. C. Phillips, A. Zobelli, I. C. Infante, E. Jacquet, V. Garcia, S. Fusil, P. R. Briddon, N. Guiblin, A. Mougin, A. A. Ünal, F. Kronast, S. Valencia, B. Dkhil, A. Barthélémy, M. Bibes, Electric-field control of magnetic order above room temperature. *Nat. Mater.* 13, 345–351 (2014).
- U. Bauer, L. Yao, A. J. Tan, P. Agrawal, S. Emori, H. L. Tuller, S. van Dijken, G. S. D. Beach, Magneto-ionic control of interfacial magnetism. *Nat. Mater.* 14, 174–181 (2015).
- S. Miwa, M. Suzuki, M. Tsujikawa, K. Matsuda, T. Nozaki, K. Tanaka, T. Tsukahara, K. Nawaoka, M. Goto, Y. Kotani, T. Ohkubo, F. Bonell, E. Tamura, K. Hono, T. Nakamura, M. Shirai, S. Yuasa, Y. Suzuki, Voltage controlled interfacial magnetism through platinum orbits. *Nat. Commun.* 8, 15848 (2017).
- S. V. Aradhya, G. E. Rowlands, J. Oh, D. C. Ralph, R. A. Buhrman, Nanosecond-timescale low energy switching of in-plane magnetic tunnel junctions through dynamic Oersted-fieldassisted spin Hall effect. *Nano Lett.* 16, 5987–5992 (2016).
- M. Baumgartner, K. Garello, J. Mendil, C. O. Avci, E. Grimaldi, C. Murer, J. Feng, M. Gabureac, C. Stamm, Y. Acremann, S. Finizio, S. Wintz, J. Raabe, P. Gambardella, Spatially and time-resolved magnetization dynamics driven by spin-orbit torques. *Nat. Nanotechnol.* 12, 980–986 (2017).
- S. Shi, Y. Ou, S. V. Aradhya, D. C. Ralph, R. A. Buhrman, Fast low-current spin-orbit-torque switching of magnetic tunnel junctions through atomic modifications of the free-layer interfaces. *Phys. Rev. Appl.* 9, 011002 (2018).
- J. Nitta, T. Akazaki, H. Takayanagi, T. Enoki, Gate control of spin-orbit interaction in an inverted In_{0.53}Ga_{0.47}As/In_{0.52}Al_{0.48}As heterostructure. *Phys. Rev. Lett.* 78, 1335–1338 (1997).
- S. Lee, H. Koike, M. Goto, S. Miwa, Y. Suzuki, N. Yamashita, R. Ohshima, E. Shigematsu, Y. Ando, M. Shiraishi, Synthetic Rashba spin–orbit system using a silicon metal-oxide semiconductor. *Nat. Mater.* 20, 1228–1232 (2021).
- Y. Fan, X. Kou, P. Upadhyaya, Q. Shao, L. Pan, M. Lang, X. Che, J. Tang, M. Montazeri, K. Murata, L.-T. Chang, M. Akyol, G. Yu, T. Nie, K. L. Wong, J. Liu, Y. Wang, Y. Tserkovnyak, K. L. Wang, Electric-field control of spin-orbit torque in a magnetically doped topological insulator. *Nat. Nanotechnol.* 11, 352–359 (2016).
- M.-G. Kang, J.-G. Choi, J. Jeong, J. Y. Park, H.-J. Park, T. Kim, T. Lee, K.-J. Kim, K.-W. Kim, J. H. Oh, D. D. Viet, J.-R. Jeong, J. M. Yuk, J. Park, K.-J. Lee, B.-G. Park, Electric-field control of field-free spin-orbit torque switching via laterally modulated Rashba effect in Pt/Co/AlO_x structures. Nat. Commun. 12, 7111 (2021).
- E. Saitoh, M. Ueda, H. Miyajima, G. Tatara, Conversion of spin current into charge current at room temperature: Inverse spin-Hall effect. Appl. Phys. Lett. 88, 182509 (2006).
- 14. L. Liu, C.-F. Pai, Y. Li, H. W. Tseng, D. C. Ralph, R. A. Buhrman, Spin-torque switching with the giant spin Hall effect of Tantalum. *Science* **336**, 555–558 (2012).
- C.-F. Pai, L. Liu, Y. Li, H. W. Tseng, D. C. Ralph, R. A. Buhrman, Spin transfer torque devices utilizing the giant spin Hall effect of tungsten. *Appl. Phys. Lett.* 101, 122404 (2012).
- D. Chiba, S. Fukami, K. Shimamura, N. Ishiwata, K. Kobayashi, T. Ono, Electrical control of the ferromagnetic phase transition in cobalt at room temperature. *Nat. Mater.* 10, 853–856 (2011).
- T. Hirai, T. Koyama, A. Obinata, Y. Hibino, K. Miwa, S. Ono, M. Kohda, D. Chiba, Control of magnetic anisotropy in Pt/Co system using ionic liquid gating. *Appl. Phys. Express* 9, 063007 (2016).
- A. J. Tan, M. Huang, C. O. Avci, F. Büttner, M. Mann, W. Hu, C. Mazzoli, S. Wilkins, H. L. Tuller, G. S. D. Beach, Magneto-ionic control of magnetism using a solid-state proton pump. *Nat. Mater.* 18, 35–41 (2019).
- G. De Simoni, F. Paolucci, P. Solinas, E. Strambini, F. Giazotto, Metallic supercurrent field-effect transistor. Nat. Nanotechnol. 13, 802–805 (2018).
- S. Dushenko, M. Hokazono, K. Nakamura, Y. Ando, T. Shinjo, M. Shiraishi, Tunable inverse spin Hall effect in nanometer-thick platinum films by ionic gating. *Nat. Commun.* 9, 3118 (2018).
- Y. Maruyama, R. Ohshima, E. Shigematsu, Y. Ando, M. Shiraishi, Modulation of Hanle magnetoresistance in an ultrathin platinum film by ionic gating. *Appl. Phys. Express* 16, 023004 (2023).
- R. Chu, L. Liu, B. Cui, W. Liu, T. An, X. Ren, T. Miao, B. Cheng, J. Hu, Electrical control of spin Hall effect in Pt by hydrogen ion adsorption and desorption. ACS Nano 16, 16077–16084 (2022).
- Y. Yan, C. Wan, X. Zhou, G. Shi, B. Cui, J. Han, Y. Fan, X. Han, K. L. Wang, F. Pan, C. Song, Strong electrical manipulation of spin–orbit torque in ferromagnetic heterostructures. Adv. Electron. Mater. 2, 1600219 (2016).
- W. Liu, L. Liu, B. Cui, S. Cheng, X. Wu, B. Cheng, T. Miao, X. Ren, R. Chu, M. Liu, X. Zhao, S. Wu, H. Qin, J. Hu, Manipulation of spin-orbit torque in tungsten oxide/manganite heterostructure by ionic liquid gating and orbit engineering. ACS Nano 17, 23626–23636 (2023).

SCIENCE ADVANCES | RESEARCH ARTICLE

- R. Mishra, F. Mahfouzi, D. Kumar, K. Cai, M. Chen, X. Qiu, N. Kioussis, H. Yang, Electric-field control of spin accumulation direction for spin-orbit torques. *Nat. Commun.* 10, 248 (2019)
- K. Ando, S. Takahashi, K. Harii, K. Sasage, J. Ieda, S. Maekawa, E. Saitoh, Electric manipulation of spin relaxation using the spin Hall effect. *Phys. Rev. Lett.* 101, 036601 (2008).
- L. Liu, T. Moriyama, D. C. Ralph, R. A. Buhrman, Spin-torque ferromagnetic resonance induced by the spin Hall effect. *Phys. Rev. Lett.* 106, 036601 (2011).
- I. M. Miron, G. Gaudin, S. Auffret, B. Rodmacq, A. Schuhl, S. Pizzini, J. Vogel, P. Gambardella, Current-driven spin torque induced by the Rashba effect in a ferromagnetic metal layer. Nat. Mater. 9, 230–234 (2010).
- U. H. Pi, K. W. Kim, J. Y. Bae, S. C. Lee, Y. J. Cho, K. S. Kim, S. Seo, Tilting of the spin orientation induced by Rashba effect in ferromagnetic metal layer. *Appl. Phys. Lett.* 97, 162507 (2010).
- M. Hayashi, J. Kim, M. Yamanouchi, H. Ohno, Quantitative characterization of the spin-orbit torque using harmonic Hall voltage measurements. *Phys. Rev. B* 89, 144425 (2014)
- J. Kim, J. Sinha, M. Hayashi, M. Yamanouchi, S. Fukami, T. Suzuki, S. Mitani, H. Ohno, Layer thickness dependence of the current-induced effective field vector in Ta|CoFeB|MgO. Nat. Mater. 12, 240–245 (2013).
- S. An, E. Baek, J.-A. Kim, K.-S. Lee, C.-Y. You, Improved spin-orbit torque induced magnetization switching efficiency by helium ion irradiation. Sci. Rep. 12, 3465 (2022).
- T. Sato, T. Maruo, S. Marukane, K. Takagi, Ionic liquids containing carbonate solvent as electrolytes for lithium ion cells. J. Power Sources 138, 253–261 (2004).
- G. Hu, G. P. Pandey, Q. Liu, R. S. Anaredy, C. Ma, M. Liu, J. Li, S. K. Shaw, J. Wu, Selforganization of ions at the interface between graphene and ionic liquid DEME-TFSI. ACS Appl. Mater. Interfaces 9, 35437–35443 (2017).
- H. Yuan, H. Shimotani, A. Tsukazaki, A. Ohtomo, M. Kawasaki, Y. Iwasa, High-density carrier accumulation in ZnO field-effect transistors gated by electric double layers of ionic liquids. Adv. Funct. Mater. 19, 1046–1053 (2009).
- M.-H. Nguyen, D. C. Ralph, R. A. Buhrman, Spin torque study of the spin Hall conductivity and spin diffusion length in platinum thin films with varying resistivity. *Phys. Rev. Lett.* 116, 126601 (2016).
- K. Y. Lee, S. Jo, A. J. Tan, M. Huang, D. Choi, J. H. Park, H. I. Ji, J. W. Son, J. Chang, G. S. D. Beach, S. Woo, Fast magneto-ionic switching of interface anisotropy using yttria-stabilized zirconia gate oxide. *Nano Lett.* 20, 3435–3441 (2020).
- S. Rüegg, G. Schütz, P. Fischer, R. Wienke, W. B. Zeper, H. Ebert, Spin-dependent x-ray absorption in Co/Pt multilayers. J. Appl. Phys. 69, 5655–5657 (1991).
- F. Wilhelm, P. Poulopoulos, A. Scherz, H. Wende, K. Baberschke, M. Angelakeris,
 N. K. Flevaris, J. Goulon, A. Rogalev, Interface magnetism in 3d/5d multilayers probed by
 X-ray magnetic circular dichroism. Phys. Status Solidi A 196, 33–36 (2003).
- M. Suzuki, H. Muraoka, Y. Inaba, H. Miyagawa, N. Kawamura, T. Shimatsu, H. Maruyama, N. Ishimatsu, Y. Isohama, Y. Sonobe, Depth profile of spin and orbital magnetic moments in a subnanometer Pt film on Co. *Phys. Rev. B.* 72, 054430 (2005).
- T. Kuschel, C. Klewe, J. M. Schmalhorst, F. Bertram, O. Kuschel, T. Schemme, J. Wollschläger, S. Francoual, J. Strempfer, A. Gupta, M. Meinert, G. Götz, D. Meier, G. Reiss, Static magnetic proximity effect in Pt/NiFe₂O₄ and Pt/Fe bilayers investigated by X-Ray resonant magnetic reflectivity. *Phys. Rev. Lett.* **115**, 097401 (2015).
- C. Klewe, T. Kuschel, J. M. Schmalhorst, F. Bertram, O. Kuschel, J. Wollschläger, J. Strempfer, M. Meinert, G. Reiss, Static magnetic proximity effect in Pt/Ni_{1-x} Fex bilayers investigated by x-ray resonant magnetic reflectivity. *Phys. Rev. B* 93, 214440 (2016).
- A. Mukhopadhyay, S. K. Vayalil, D. Graulich, I. Ahamed, S. Francoual, A. Kashyap, T. Kuschel, P. S. A. Kumar, Asymmetric modification of the magnetic proximity effect in Pt/Co/Pt trilayers by the insertion of a Ta buffer layer. *Phys. Rev. B* 102, 144435 (2020).
- D. Graulich, J. Krieft, A. Moskaltsova, J. Demir, T. Peters, T. Pohlmann, F. Bertram, J. Wollschläger, J. R. Jose, S. Francoual, T. Kuschel, Quantitative comparison of the magnetic proximity effect in Pt detected by XRMR and XMCD. *Appl. Phys. Lett.* 118, 012407 (2021)
- 45. Y. Ebisuzaki, W. J. Kass, M. O'Keeffe, Solubility and diffusion of hydrogen and deuterium in platinum. *J. Chem. Phys.* **49**, 3329–3332 (1968).

- K. Tsukada, H. Inoue, F. Katayama, K. Sakai, T. Kiwa, Changes in work function and electrical resistance of Pt thin films in the presence of hydrogen gas. *Jpn. J. Appl. Phys.* 51, 015701 (2012).
- T. Toya, Theory of hydrogen adsorption on platinum. J. Res. Inst. Catalysis Hokkaido Univ. 10, 236–260 (1962).
- X. Qiu, W. Legrand, P. He, Y. Wu, J. Yu, R. Ramaswamy, A. Manchon, H. Yang, Enhanced spin-orbit torque via modulation of spin current absorption. *Phys. Rev. Lett.* 117, 217206 (2016).
- M. Aoki, Y. Yin, S. Granville, Y. Zhang, N. V. Medhekar, L. Leiva, R. Ohshima, Y. Ando, M. Shiraishi, Gigantic anisotropy of self-induced spin-orbit torque in Weyl ferromagnet Co₂MnGa. *Nano Lett.* 23, 6951–6957 (2023).
- E. Sagasta, Y. Omori, M. Isasa, M. Gradhand, L. E. Hueso, Y. Niimi, Y. Otani, F. Casanova, Tuning the spin Hall effect of Pt from the moderately dirty to the superclean regime. *Phys. Rev. B* 94, 060412 (2016).
- H. Kontani, M. Naito, D. S. Hirashima, K. Yamada, J. Inoue, Study of intrinsic spin and orbital Hall effects in Pt based on a (6s, 6p, 5d) tight-binding model. *J. Physical Soc. Japan* 76, 103702 (2007).
- T.Tanaka, H. Kontani, M. Naito, T. Naito, D. S. Hirashima, K. Yamada, J. Inoue, Intrinsic spin Hall effect and orbital Hall effect in 4d and 5d transition metals. *Phys. Rev. B* 77, 165117 (2008).
- H. Kontani, T. Tanaka, D. S. Hirashima, K. Yamada, J. Inoue, Giant orbital Hall effect in transition metals: Origin of large spin and anomalous Hall effects. *Phys. Rev. Lett.* 102, 016601 (2009).
- G. Y. Guo, S. Murakami, T. W. Chen, N. Nagaosa, Intrinsic spin Hall effect in platinum: First-principles calculations. *Phys. Rev. Lett.* 100, 096401 (2008).
- C. F. Pai, M. Mann, A. J. Tan, G. S. D. Beach, Determination of spin torque efficiencies in heterostructures with perpendicular magnetic anisotropy. *Phys. Rev. B* 93, 144409 (2016).
- A. T. Wong, J. H. Noh, P. R. Pudasaini, B. Wolf, N. Balke, A. Herklotz, Y. Sharma, A. V. Haglund,
 Dai, D. Mandrus, P. D. Rack, T. Z. Ward, Impact of gate geometry on ionic liquid gated ionotronic systems. APL Mater. 5, 042501 (2017).
- H. An, H. Nakayama, Y. Kanno, A. Nomura, S. Haku, K. Ando, Spin-orbit torques in asymmetric Pt/Co/Pt structures. *Phys. Rev. B* 94, 214417 (2016).
- T. Valet, A. Fert, Theory of the perpendicular magnetoresistance in magnetic multilayers. Phys. Rev. B 48, 7099–7113 (1993).
- M. Althammer, S. Meyer, H. Nakayama, M. Schreier, S. Altmannshofer, M. Weiler, H. Huebl,
 Geprägs, M. Opel, R. Gross, D. Meier, C. Klewe, T. Kuschel, J.-M. Schmalhorst, G. Reiss,
 L. Shen, A. Gupta, Y.-T. Chen, G. E. W. Bauer, E. Saitoh, S. T. B. Goennenwein, Quantitative study of the spin Hall magnetoresistance in ferromagnetic insulator/normal metal hybrids. *Phys. Rev. B* 87, 224401 (2013).
- K. Roy, Estimating the spin diffusion length and the spin Hall angle from spin pumping induced inverse spin Hall voltages. Phys. Rev. B 96, 174432 (2017).
- S. Okamoto, K. Nishiyama, O. Kitakami, Y. Shimada, Enhancement of magnetic surface anisotropy of Pd/Co/Pd trilayers by the addition of Sm. J. Appl. Phys. 90, 4085–4088 (2001).

Acknowledgments

Funding: This research was supported by the National Research Foundation of Korea (NRF-2021M3F3A2A01037525). Author contributions: Conceptualization: S.L. and C.-Y.Y. Methodology: S.L., D.K., and J.C. Investigation: S.L., D.K., and J.C. Data curation: S.L. Formal analysis: S.L., S.A., E.B., and C.-Y.Y. Supervision: S.L. and C.-Y.Y. Visualization: S.L. Writing—original draft: S.L. and C.-Y.Y. Writing—review and editing: S.L., S.A., E.B., D.K., J.C., and C.-Y.Y. Competing interests: S.L. and C.-Y.Y. are inventors on the following patents related to this work: Korean patent (patent no. 10-2626970, granted on 16 January 2024), PCT patent application (application no. PCT/KR2022/021087, filed on 22 December 2022), and US patent application (application no. 18/701,715, now under examination). The authors declare that they have no other competing interests. Data and materials availability: All data needed to evaluate the conclusions in the paper are present in the paper and/or the Supplementary Materials.

Submitted 12 June 2024 Accepted 11 February 2025 Published 19 March 2025 10.1126/sciadv.adr0457